Ocean Engineering 82 (2014) 42–51

Contents lists available at ScienceDirect

Ocean Engineering

journal homepage: www.elsevier.com/locate/oceaneng

# Wave-energy dissipation by bottom friction in the English Channel

Nicolas Guillou

*Laboratoire de Génie Côtier et Environnement (LGCE), Cerema/DTecEMF/DS, 155 rue Pierre Bouguer Technopôle Brest-Iroise, BP 5, 29280 Plouzané, France*

ARTICLE INFO

*Article history:*
Received 1 August 2013
Accepted 17 February 2014
Available online 15 March 2014

*Keywords:*
Modelling
Bottom-drag coefficient
SWAN
English Channel
Le Havre
Cherbourg

ABSTRACT

The energy dissipation by bottom friction of wind-generated surface-gravity waves is evaluated in relation to the seabed roughness magnitude in the English Channel (western Europe). The investigation is based on the phase-averaged wave model SWAN (Simulating WAves Nearshore) modified to account for a new parameterisation of the wind-drag coefficient at high wind speeds. Two formulations of the bottom-drag coefficient are evaluated: (1) the default constant empirical values derived from the JONSWAP experiment and (2) the eddy-viscosity model of Madsen et al. (1988) integrating the hydrodynamic conditions and the bottom roughness length scale considered successively constant and parametrised according to the grain size of bed sediments. Model performances are evaluated by comparing predictions with available measurements of the significant wave height and the peak period at (1) three offshore lightships and (2) two nearshore wave buoys off Le Havre and Cherbourg harbours. The heterogeneous bottom roughness length scale associated with the grain size of seabed sediments improves globally numerical estimates. Mappings of coastal regions influenced by bottom friction are produced exhibiting significant energy dissipation in areas of pebbles and gravels of the Normano-Breton Gulf and the surroundings of the Isle of Wight exposed to the incoming waves from the North-Atlantic ocean.



## 1. Introduction

Refined estimations of the transformation of wind-generated surface-gravity waves in shelf environments are crucial for many offshore and coastal engineering applications dealing with the safety and reliability of marine structural mechanics, the exploitation of waves renewable energy or the design of harbours and waterfronts. Among the different dissipation and dispersion mechanisms of wave energy in coastal waters (*e.g.*, refraction, diffraction shoaling, etc.), seabed interaction processes may be significant in nearshore areas leading to a substantial decrease by 40–50% of the wave height during extreme storm events such as hurricanes (*e.g.*, Riedel et al., 2005; Siadatmousavi et al., 2011).

The interaction between the surface waves and the sea bed can appear in different ways depending in particular on bottom conditions. These processes reviewed by Shemdin et al. (1978) include percolation into a porous bottom, motion of a soft muddy bed, scattering on bottom irregularities and friction created by the orbital motion of water particles under wave conditions. In many continental shelves covered by sandy bottoms, bed friction is considered to be the dominant mechanism (*e.g.*, Shemdin et al., 1978; Bertotti and Cavaleri, 1994).

In the energy balance equation of third-generation wave models, this dissipation process is integrated using the formulation proposed by Weber (1991a,b) introducing a bottom-friction coefficient determined by the hydrodynamics, the bottom topography and the bed roughness. Numerous formulations have been proposed to approach this coefficient ranging from empirical constant values (*e.g.*, Hasselmann et al., 1973; Bouws and Komen, 1983) traditionally implemented in operational applications (*e.g.*, Komen et al., 1994) to more complicated models integrated the effects of wave-induced bottom velocity and bed-sediment properties (*e.g.*, Hasselmann and Collins, 1968; Collins, 1972; Madsen et al., 1988). Detailed reviews have been established by Luo and Monbaliu (1994) or the WISE Group (2007). Nevertheless, given the lack of information on bottom materials, the nature and properties of bottom sediments were considered in few applications (*e.g.* Ardhuin et al., 2003a,b; Siadatmousavi et al., 2011).

The present study extends these numerical investigations evaluating the effects of bed-sediment grain-size distributions and associated sand ripples features on wave-energy dissipation by bottom friction. The site of application is the English Channel (western Europe) (Fig. 1). This shelf environment is occasionally subjected to storm events with a significant wave height reaching 5 m at its western entrance for around 5% of the time (*e.g.*, Benoit and Lafon, 2004). It presents furthermore a highly heterogeneous spatial distribution of bottom sediments with (1) very fine sands,

*E-mail address:* nicolas.guillou@cerema.fr

http://dx.doi.org/10.1016/j.oceaneng.2014.02.029
0029-8018 

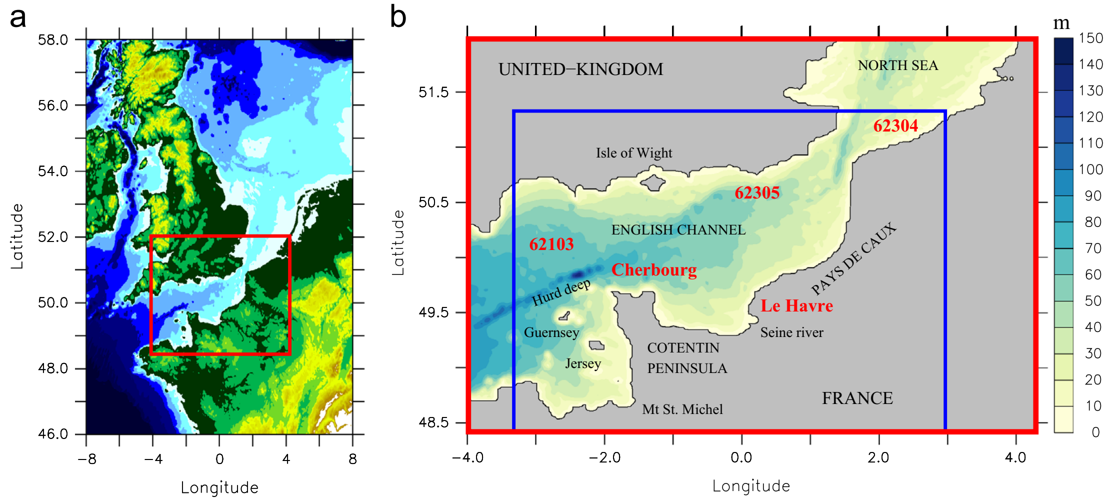


**Fig. 1.** (a) Location of the English Channel in the North-western European continental shelf, (b) bathymetry of the computational domain with the locations of the measurement points. The blue rectangle shows the area where the spatial heterogeneous bottom roughness is introduced. (For interpretation of the references to colour in this figure caption, the reader is referred to the web version of this paper.)

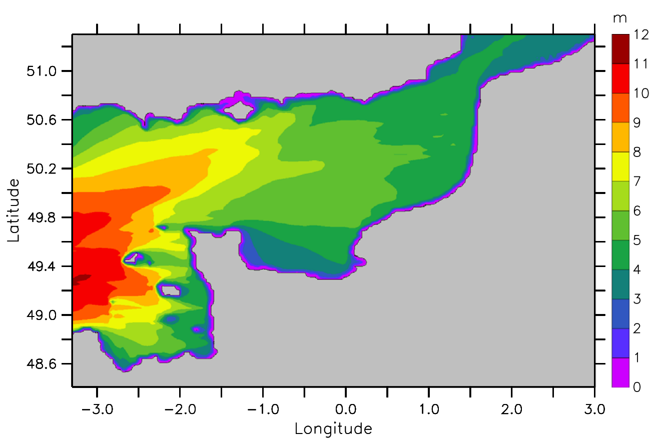


**Fig. 2.** Maximum significant wave height predicted in March 2008 in the English Channel.

silts and muds in bays and estuaries and (2) pebbles and gravels in the Dover Strait, off the “Pays de Caux” and over an extensive zone in the central Channel between the Isle of Wight and the Cotentin Peninsula (Vaslet et al., 1979; Larsonneur et al., 1982).

The approach retained here relies on a comparison between numerical predictions and observations of the significant wave height and the peak period. Available field measurements are realised at three offshore lightships and two nearshore wave buoys off Le Havre and Cherbourg harbours (Fig. 1b, Section 2.1). Modelling is based on the phase-averaged wave model SWAN (Simulating WAves Nearshore) (version 40.85) (Booij et al., 1999) modified to account for a new parameterisation of the wind-drag coefficient at high wind speeds (Section 2.2). A pre-processing module computes the required surficial sediment granulometric distribution from a series of bottom samples and the associated heterogeneous frictional parameters (Section 2.3). Numerical predictions are compared with observations over the period from December 2007 to March 2008 characterised by an extreme storm event on 10 March 2008 with significant wave heights over 10 m at the western entrance of the English Channel (Fig. 2) (Section 3.1). A preliminary study compares first model performances with (1) the default wind-drag coefficient proposed in SWAN and (2) the new formulation (Section 3.2.1). The effects of a heterogeneous seabed roughness magnitude are then evaluated confronting predictions obtained with (1) constant empirical values of the bottom-friction coefficient proposed by Hasselmann et al. (1973) and Bouws and Komen (1983) and (2) the eddy-viscosity model of Madsen et al. (1988) which integrates hydrodynamics and seabed roughness magnitude (Section 3.2.2). Mappings of numerical predictions are finally produced over the entire computational domain to encompass the spatial and temporal changes of (1) the significant wave height and (2) the bottom-dissipation coefficient with respect to constant default values (Section 3.3).

## 2. Materials and methods

### 2.1. Measurements

A series of 2318 bottom sediment samples have been collected from 1971 to 1976 in the framework of the “RCP 378 Benthos de la Manche” program (Cabioch et al., 1977) to characterise the spatial distribution of bed-sediments grain sizes in the English Channel. Samples were passed through a series of nine standard AFNOR (Association Française de NORmalisation) sieves ranging from 50 µm to 2 cm. The 10 corresponding classes are supplemented by a virtual class between 5.5 and 50 cm to account for boulders and rock outcrops. Further details about the resulting discretised granulometric distribution are available in Guillou and Chapalain (2010).

Available wave measurements here used were obtained at the three offshore lightships 62103, 62305 and 62304 of the UK Meteorological Office and the two nearshore wave buoys off Le Havre and Cherbourg harbours of the French CANDHIS database (Centre d'Archivage National de Données de Houle In Situ, Cerema) (Fig. 1 and Table 1). The instrumentation network is deployed in water depths ranging from 19 m at the wave buoy of Le Havre to 70 m at the lightship 62103.

### 2.2. Model

SWAN solves the time-dependent spectral action balance equation (*e.g.*, Mei, 1983; Komen et al., 1994) ignoring the modifications of waves components by the ambient current and the free-surface elevation whereas it can handle these effects

$$\frac{\partial N}{\partial t} + \nabla_{\mathbf{x}} \cdot [\mathbf{c_g} N] + \frac{\partial c_\sigma N}{\partial \sigma} + \frac{\partial c_\theta N}{\partial \theta} = \frac{S_{tot}}{\sigma} \quad (1)$$

where $t$ denotes times, $\nabla_{\mathbf{x}}$ is the horizontal gradient operator and $N$ is the action density defined as $N = E/\sigma$ with $E$ being the wave

**Table 1**
Coordinates and water depths at the five measurement sites.

| Measurement sites | Long. | Lat. | Water depth (m) |
|---|---|---|---|
| 62103 | 2.90°W | 49.90°N | 70 |
| 62305 | 0.00°W | 50.40°N | 55 |
| 62304 | 1.80°E | 51.10°N | 26 |
| Le Havre | 0.16°W | 49.52°N | 19 |
| Cherbourg | 1.62°W | 49.70°N | 23 |

energy density distributing over intrinsic frequencies $\sigma$ and propagation directions $\theta$. $\mathbf{c_g}$ denotes the group velocity while quantities $c_\sigma$ and $c_\theta$ are the propagation velocities in spectral space $(\sigma, \theta)$. $S_{tot}$ contains the source and sink terms of physical processes which generate, dissipate or redistribute wave energy like non-linear transfer of energy through wave–wave interactions or wave–energy dissipation due to whitecapping, bottom friction and depth-induced breaking. The parameterisation adopted for sources and sinks terms are briefly detailed hereafter with a focus on the energy dissipation induced by bottom friction.

Energy dissipation in random waves due to depth-induced breaking is quantified according to Battjes and Janssen (1978).

Wave growth by wind is computed with the exponential term of Komen et al. (1984). Two formulations are considered for the wind-drag coefficient $C_d$:

(1) the default expression proposed in SWAN and based on Wu (1982)

$$C_d = \begin{cases} 1.2875 \times 10^{-3} & \text{for } u_{10} < 7.5 \text{ m s}^{-1} \\ (0.8 + 0.065 u_{10}) \times 10^{-3} & \text{for } u_{10} \geq 7.5 \text{ m s}^{-1} \end{cases} \tag{2}$$

and (2) the new relationship recently derived by Zijlema et al. (2012) to fit a compilation of observations at high wind speeds

$$C_d = \left( 0.55 + 2.97 \left( \frac{u_{10}}{u_{ref}} \right) - 1.49 \left( \frac{u_{10}}{u_{ref}} \right)^2 \right) \times 10^{-3} \tag{3}$$

where $u_{10}$ is the wind-speed amplitude at 10 m above the free surface and $u_{ref}$ is the reference wind amplitude taken equal to $u_{ref} = 31.5$ m s$^{-1}$.

Processes of whitecapping are described with the pulse-model equation of Hasselmann (1974) retaining original coefficients proposed by Komen et al. (1984).

The sink term of energy dissipation by bottom friction is computed according to the following formulation:

$$S_{ds,b} = -C_b \frac{\sigma^2}{g^2 \sinh^2(kd)} E(\sigma, \theta) \tag{4}$$

where $k$ is the wave number of the spectral component, $d$ is the water depth and $g$ is the acceleration of gravity taken equal to $g = 9.81$ m s$^{-2}$. Two formulations are considered for the computation of the bottom-friction coefficient $C_b$. The first parameterisation here retained consists in prescribing constant empirical values. In the JONSWAP experiment, Hasselmann et al. (1973) suggested to use a value of $C_b = 0.038$ m$^2$ s$^{-3}$ for swell dissipation over sandy bottoms. This value was re-examined by Bouws and Komen (1983) for fully developed wind seas as $C_b = 0.067$ m$^2$ s$^{-3}$. The second parameterisation follows Madsen et al. (1988) who derived a formulation which integrates the effects of hydrodynamics and bed roughness. The bottom-friction coefficient is given by

$$C_b = f_\omega \frac{g}{\sqrt{2}} U_{rms} \tag{5}$$

where $U_{rms}$ is the root mean square bottom-orbital velocity. $f_\omega$ is the non-dimensional friction factor estimated with the formulation proposed by Jonsson (1966)

$$\frac{1}{4\sqrt{f_\omega}} + \log_{10}\left( \frac{1}{4\sqrt{f_\omega}} \right) = m_f + \log_{10}\left( \frac{a_b}{k_n} \right) \tag{6}$$

where $m_f$ is taken equal to $m_f = -0.08$ according to Jonsson and Carlsen (1976), $a_b$ is the representative near-bottom excursion amplitude and $k_n$ is the bottom roughness length scale. This formulation is retained when the condition $a_b/k_n > 1.57$ is satisfied. For values $a_b/k_n < 1.57$, $f_\omega$ is taken equal to $f_\omega = 0.3$. The bottom roughness length scale is determined by bed-sediments grain sizes and the presence or not of sand ripples. Bed features may form on sandy beds with median diameters $D_{50} < 800$ μm (*e.g.*, Soulsby, 1997). In the present investigation, sea beds made of coarser sediments (*i.e.*, $D_{50} > 800$ μm) remain thus featureless with a roughness length scale equals to $k_n = 3D_{90}$, where $D_{90}$ is the grain diameter for which 90% of the grains by mass is finer (Van Rijn, 1993). If sandy beds ($D_{50} < 800$ μm) are considered featureless, the bottom roughness length scale is taken equal to the grain-related component $k_n = 2.5D_{50}$ (*e.g.*, Soulsby, 1997). If sandy ripples are considered, the associated roughness parameter $k_n$ is modified for median diameters $D_{50} < 800$ μm. Whereas numerous algorithms have been developed to integrate the effects of wave-ripples generation in numerical models (*e.g.*, Graber and Madsen, 1988; Tolman, 1994; Ardhuin et al., 2003a; Smith et al., 2011), the present investigation is restricted to the consideration of current-induced ripples to integrate the strong influence of tidal currents on sediment transport in the English Channel (*e.g.*, Guillou et al., 2009; Guillou and Chapalain, 2010). As a first estimate of the effects of a heterogeneous seabed roughness magnitude on wave conditions, more complex predictors of sand ripple geometry under the combined influence of tidal current and waves (*e.g.*, Li and Amos, 1998, 2001) are ignored. The roughness length scale associated with the presence of sand ripples is parametrised according to Wooding et al. (1973) and Yalin (1985) resulting in values of $k_n \simeq 240D_{50}$. This relationship is consistent with the linear formulation recently proposed by Siadatmousavi et al. (2011): $k_n = 200D_{50}$.

The wave action balance equation is expressed in a spherical coordinate system. The SWAN time-dependent spectral action balance equation is solved on a regular grid, a constant directional resolution and an exponential frequency distribution with an implicit time discretisation Euler technique. Further details about the mathematical expressions of sources and sinks are available in SWAN technical documentation (SWAN team, 2009).

### 2.3. Setup

SWAN is set up on a computational domain covering the English Channel between longitudes 4.000°W and 4.291°E and latitudes 48.410°N and 51.992°N (Fig. 1). It is discretised on a 280 × 200 horizontal grid with a spacing of 2 km. The model runs with 30 exponentially spaced frequencies ranging from 0.05 to 1 Hz, 60 evenly spaced directions (6° resolution) and a time step of 10 min. Wind velocity components at 10 m above the free surface are provided by the meteorological model ALADIN (Aire Limitée, Adaptation dynamique, Développement InterNational, Bénard, 2004, MétéoFrance). SWAN is driven by the wave components predicted along each open boundary from a regional run of WaveWatch III on the North-western European continental shelf in the context of the IOWAGA project (http://wwz.ifremer.fr/iowaga/Products). The heterogeneous spatial distributions of diameters $D_{50}$ and $D_{90}$ are computed in an inner domain extended in longitude from 3.300°W to 3.000°E and in latitude from 48.410°N to 51.300°N where bottom-sediments samples are available (Section 2.1, Fig. 1b). The interpolation of the observed granulometric distributions at the computational grid nodes is performed

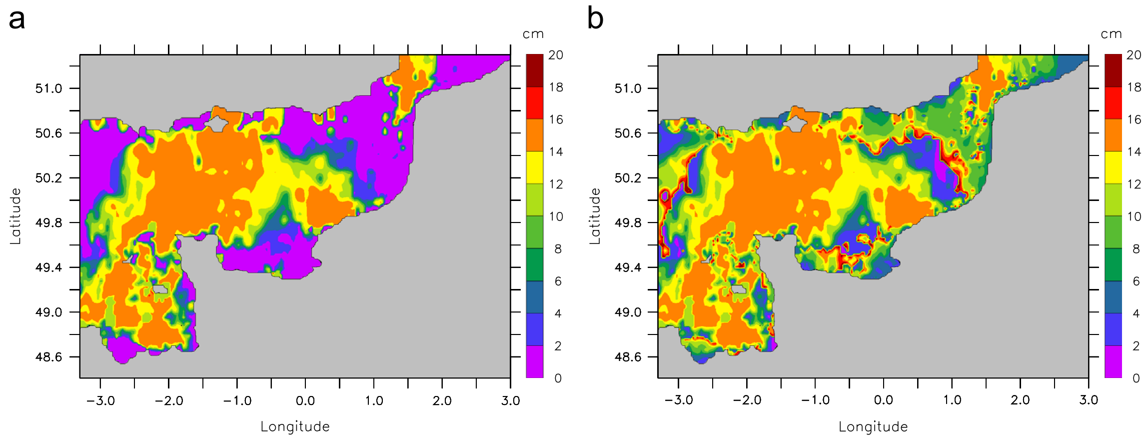


**Fig. 3.** Spatial heterogeneous bottom roughness length scale $k_n$ in the inner computational domain (a) without and (b) with bottom sand ripples.

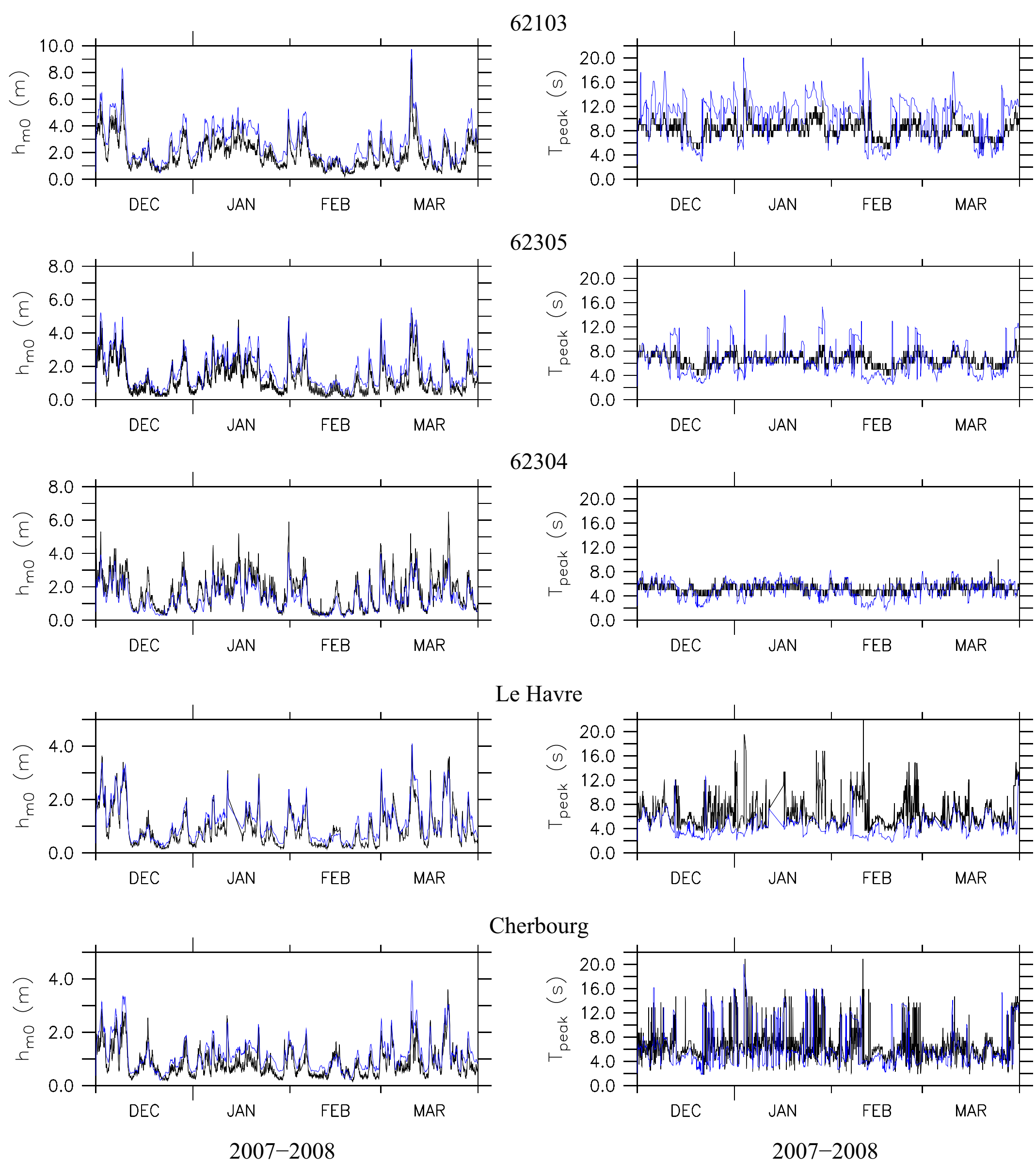


**Fig. 4.** Time series of the (black line) observed and (blue line) predicted (from configuration A1) significant wave height and peak period at offshore and nearshore measurement points in December 2007–March 2008. (For interpretation of the references to colour in this figure caption, the reader is referred to the web version of this paper.)

with the statistical mixed SFA-kriging (spherical factor analysis) method proposed by Leprêtre et al. (2006). Further details about the application of this method in the English Channel are available in Guillou (2007) and Guillou and Chapalain (2010). The resulting spatial heterogeneous bottom roughness length scales without and with the presence of sand ripples are displayed in Fig. 3a and b, respectively. $k_n$ increases significantly with the presence of sand ripples reaching values over 10 cm in bays and estuaries as well as in the eastern English Channel. Outside of this inner domain, $k_n$ is set to its default value in SWAN $k_n = 0.05$ m (SWAN team, 2009). This value falls in the range of uniform constant roughness length scales between 2 and 5 cm found to give satisfactory agreement between numerical results and measurements of the non-dimensional wave height and period (Tolman, 1991).

The wave model is run over the period from December 2007 to March 2008 when continuous observations of wave conditions in winter were available at the five measurement sites (Fig. 4). This period is characterised by the succession of six major storm events with an averaged significant wave height of 3.5 m in the central English Channel. It presents also an extreme storm event on 10 March 2008 with wave heights exceeding 10 m at the western entrance of the English Channel (Fig. 2). In order to assess model performances reached with the wind-drag formulations of Wu (1982) and Zijlema et al. (2012), four numerical experiments titled A1–A4 are conducted restricting parameterisations of the bottom-drag coefficient to constant default empirical values proposed by Hasselmann et al. (1973) and Bouws and Komen (1983) (Table 2). The influences of bottom-friction formulations are evaluated on the basis of six experiments titled B1–B3c. Experiment B1 neglects the wave energy dissipation by bottom friction. Experiments B2a and B2b consider constant bottom-friction coefficients set to values prescribed by Hasselmann et al. (1973) ($C_b = 0.038$ m$^2$ s$^{-3}$) and Bouws and Komen (1983) ($C_b = 0.067$ m$^2$ s$^{-3}$), respectively. Experiments B3a–B3c follow the parameterisation of Madsen et al. (1988). The associated bottom roughness length scale is successively considered uniform set to its default value in SWAN $k_n = 0.05$ m (SWAN team, 2009) (experiment B3a) and spatially heterogeneous neglecting (experiment B3b) and integrating (experiment B3c) sand ripples (Fig. 3a and b). These numerical experiments are compared with the standard statistical parameters of the averaged and maximum absolute differences, the scatter index

$$\mathrm{si} = \frac{\mathrm{rmse}}{(\overline{X}\,\overline{Y})^{1/2}} \tag{7}$$

with rmse being the root mean square error

$$\mathrm{rmse} = \left[\frac{1}{N}\sum_{i=1}^{i=N}(y_i - x_i)^2\right]^{1/2} \tag{8}$$

and the index of agreement introduced by Willmott (1981) as

$$\mathrm{re} = 1 - \frac{\sum_{i=1}^{i=N}|y_i - x_i|^2}{\sum_{i=1}^{i=N}(|y_i - \overline{X}| + |x_i - \overline{X}|)^2} \tag{9}$$

**Table 2**
List of numerical experiments for the estimation of wind-drag formulations.

| Numerical experiments | Bottom-drag formulations | | Wind-drag formulations | |
|---|---|---|---|---|
| | $C_b = 0.067$ m$^2$ s$^{-3}$ | $C_b = 0.038$ m$^2$ s$^{-3}$ | Wu (1982) | Zijlema et al. (2012) |
| A1 | X | | X | |
| A2 | | X | X | |
| A3 | X | | | X |
| A4 | | X | | X |

where $N$ is the number of data in the discretised time series considered, $(x_i)$ and $(y_i)$ represent the two sets of measured and simulated values and $\overline{X}$ and $\overline{Y}$ are respectively the averaged of the observations $(x_i)$ and predictions $(y_i)$ over the time period considered. The relative error varies between 0 and 1. It equals to unity for perfect agreement.

## 3. Results and discussion

### *3.1. Comparisons with point measurements*

Fig. 4 displays the observed and predicted from configuration A1 time series of the significant wave height and peak period at offshore and nearshore measurement points in December 2007–March 2008.

The model reproduces fairly well the evolution of the significant wave height with a minimum index of agreement of 0.89 at the wave buoy of Cherbourg. Predictions approach also at the five sites considered the magnitude of the storms heights in early December, January and March 2008. Best estimates are obtained at the wave buoy of Le Havre with a relative error of 0.96. Whereas predictions tend to overestimate measurements at lightships 62103 and 62305 and the wave buoy of Cherbourg, numerical results at lightship 62304 located in the eastern English Channel appear to underestimate slightly observations.

Modelling in configuration A1 results however in greater differences with the evolution of the peak period with a maximum index of agreement of 0.67 at the lightship 62304. Whereas numerical results show nearly the same differences with measurements at the lightship 62305 and the wave buoy of Cherbourg, further differences are obtained at the lightship 62103 and the wave buoy of Le Havre. These differences are exhibited at the wave buoy of Le Havre where the sharp transitions of the peak period observed in early January and February 2008 are slightly reproduced.

### *3.2. Improvements of numerical predictions*

#### *3.2.1. Sensitivity to wind-drag formulation*

Fig. 5 portrays the scatter index and the index of agreement in predictions of the significant wave height and the peak period for the four numerical experiments A1–A4 at the five measurement points during the period of simulation.

Best estimates of the significant wave height are obtained globally with the formulation of Zijlema et al. (2012) for the two parameterisations of the bottom-friction coefficient considered. Improvements of numerical predictions are the most noticeable at point 62305 where the index of agreement is increasing from 0.90 in experiment A1 to 0.92 in configuration A3. These results are partly explained by the better agreement of Zijlema et al.'s (2012) formulation with observations of wind-drag coefficients than the expression of Wu (1982). The new formulation tends however to increase the differences at the lightship 62304. Indeed, lower $C_d$ values are obtained with this new formulation than with the original expression (Fig. 6). During the period of simulation, these differences are exhibited at high wind speeds over 15% with wind-drag coefficients reduced by 10–30% with the new formulation. For the same dissipation coefficient by bottom friction, lower significant wave heights are thus obtained with the formulation of Zijlema et al. (2012). As initial predictions from configuration A1 (Fig. 4) tend to underestimate measurements at lightship 62304, the new wind-drag coefficient increases these differences. Nevertheless, wave-energy balance at this measurement point appears consistent with conclusions of Zijlema et al. (2012) for locally generated waves during the severe Texel storm in the southern

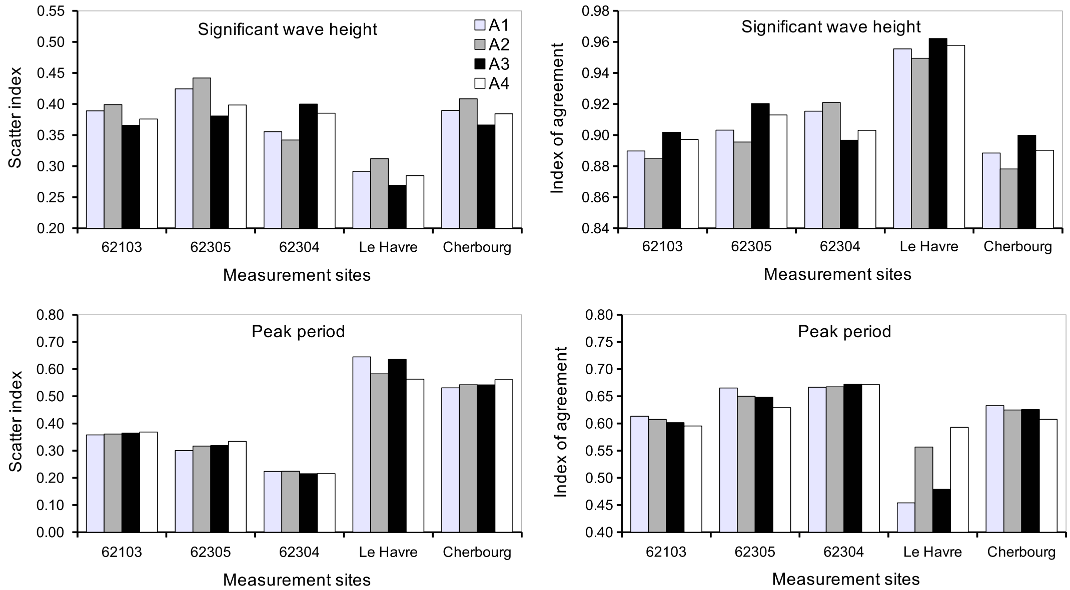


**Fig. 5.** (Left) Scatter index and (right) index of agreement in predictions of (top) the significant wave height and (bottom) the peak period at the five measurement points considered for the four numerical experiments A1–A4.

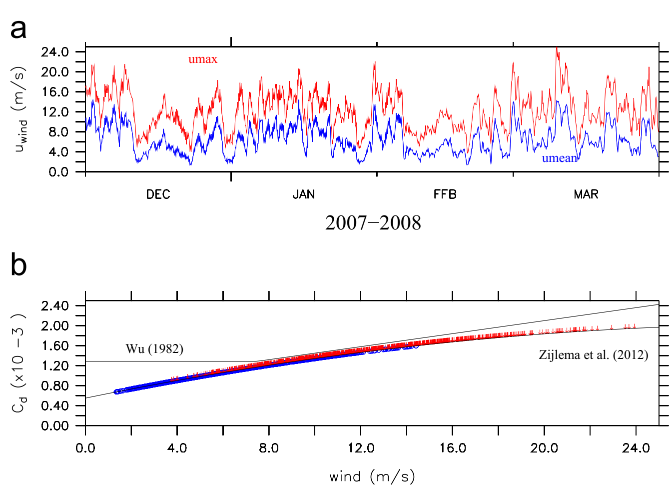


**Fig. 6.** Time series of (a) the averaged and maximum wind-speed amplitude predicted by the ALADIN meteorological model over the SWAN computational domain in December 2007–March 2008 and (b) the associated evolution of wind-drag coefficients obtained with the formulations of Wu (1982) and Zijlema et al. (2012).

North Sea. The new wind-drag coefficient gives the best estimates with the lowest friction ($C_b = 0.038$ m$^2$ s$^{-3}$). This may be related to stronger wind seas in this area than in the central or western English Channel. For the four remaining measurement sites, the best estimates of the significant wave height are reached with the new wind-drag formulation and the highest bottom friction proposed by Bouws and Komen (1983) ($C_b = 0.067$ m$^2$ s$^{-3}$).

Whereas slightly degraded predictions of the peak period are obtained with the new wind-drag formulation at offshore measurement sites and the wave buoy of Cherbourg, the expression proposed by Zijlema et al. (2012) is found to improve numerical estimates at the wave buoy of Le Havre. The index of agreement is thus increasing from 0.55 in configuration A2 to 0.59 in configuration A4. At this point, the sensitivity to wind-drag formulation is found to increase by decreasing the bottom-friction coefficient which suggests a non-negligible influence of wind on swell propagating towards the wave buoy of Le Havre.

### *3.2.2. Sensitivity to the heterogeneous bed roughness*

The sensitivity of model predictions to bottom-friction formulations is evaluated retaining the expression of Zijlema et al. (2012) for the wind-drag coefficient $C_d$. Figs. 7a,b and 8a,b display the scatter index and the index of agreement in predictions of the significant wave height and the peak period for the six numerical experiments titled B1–B3c at the lightship 62305 and the wave buoys of Le Havre and Cherbourg during the period of simulation. Predictions at lightships 62103 and 62304 are not considered because of the proximity of these measurement points to the boundaries of the inner domain where the heterogeneous bottom roughness length scale is introduced.

The consideration of wave-energy dissipation by bottom friction improves globally the numerical estimates of the significant wave height (Fig. 7a and b). At the wave buoy of Cherbourg, the scatter index is thus decreasing from 0.41 in experiment B1 to 0.34 in configuration B3c while the index of agreement is increasing from 0.87 to 0.91. These results are associated with a substantial effect of bottom friction on the significant wave height particularly noticeable during storm conditions. During the storms of December 2007 and March 2008, predicted values at the three measurement points are thus decreasing by 10–15% on average by integrating wave-energy dissipation by bottom friction (Fig. 9). The decrease of the significant wave height is particularly noticeable at the wave buoy of Le Havre where it reaches 22% during the storm of 10 March 2008. The influence of bottom friction is exhibited when computing the statistical parameters for severe conditions characterised by wave heights over 1 m (Fig. 7c and d). This overall reduction of the significant wave height improves the numerical results reducing the tendency of predictions to overestimate measurements (Section 3.1). Predictions obtained with the constant empirical value of Bouws and Komen (1983) (B2b) are furthermore very close to numerical results issued from the formulation of Madsen et al. (1988) integrating the default roughness length scale of $k_n = 0.05$ m (B3a). This is consistent with the estimation of wave models performance by Tolman (1991) who found satisfactory results for $k_n$ in the range of 2–5 cm. When compared to configuration B3a, the integration of the grain-size distribution of bottom sediments (B3b) improves also the numerical estimates at the lightship 62305 and the wave buoy of Cherbourg. Predictions at the wave buoy of Le Havre are however

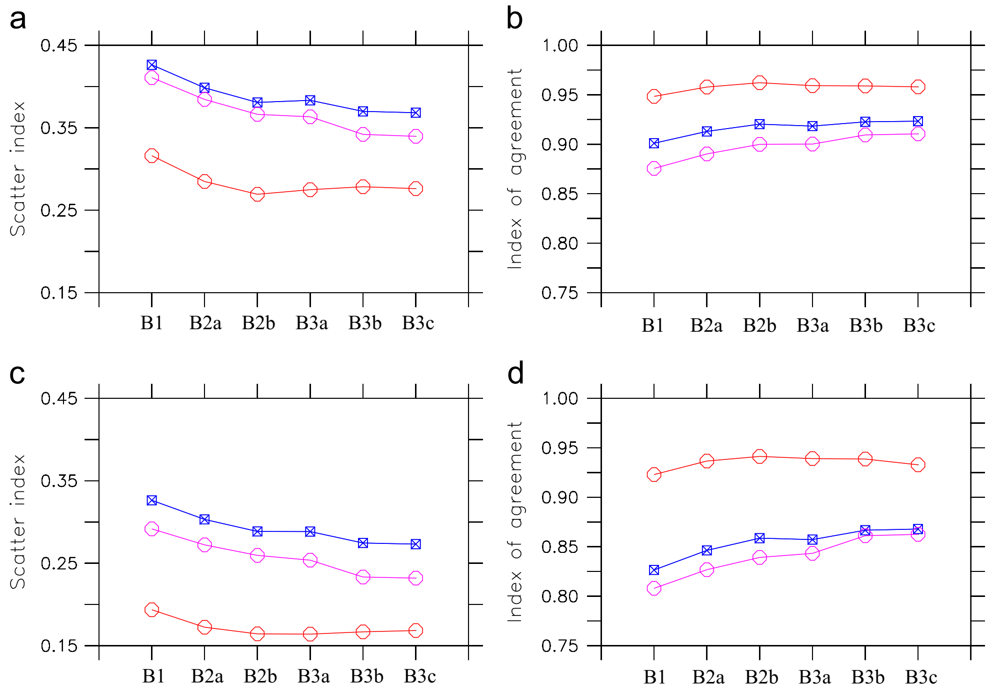


**Fig. 7.** Scatter index and index of agreement in predictions of the significant wave height at (blue) lightship 62305 and wave buoys of (red) Le Havre and (magenta) Cherbourg for the six numerical experiments B1–B3c (a, b) retaining the overall predictions and (c,d) restricting the comparison to observed wave heights over 1 m. (For interpretation of the references to colour in this figure caption, the reader is referred to the web version of this paper.)

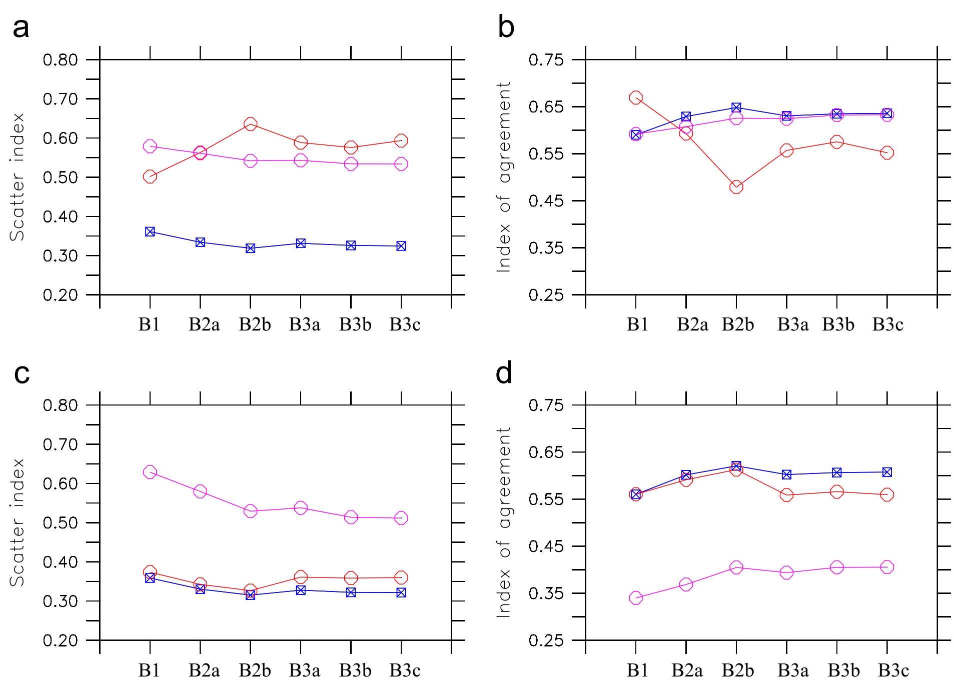


**Fig. 8.** Scatter index and index of agreement in predictions of the peak period at (blue) lightship 62305 and wave buoys of (red) Le Havre and (magenta) Cherbourg for the six numerical experiments B1–B3c (a,b) retaining the overall predictions and (c,d) restricting the comparison to observed peak period below 8 s. (For interpretation of the references to colour in this figure caption, the reader is referred to the web version of this paper.)

hardly modified. This may be related to the fact that the surrounding values of $k_n$ displayed in Fig. 3 are close to the uniform value adopted in configuration B3a. This suggests a major influence of local bottom roughness on predictions at the wave buoy of Le Havre.

Improved estimates of the peak period are also obtained at the lightship 62305 and the wave buoy of Cherbourg (Fig. 8a and b) confirming globally conclusions established for the significant wave height. The quality of predictions at the wave buoys of Le Havre appears however to deteriorate when increasing the bottom-friction coefficient. The index of agreement is thus decreasing from 0.67 when bottom friction is neglected (B1) to 0.48 when the bottom-drag coefficient of Bouws and Komen (1983) ($C_b = 0.067\ \mathrm{m}^2\ \mathrm{s}^{-3}$) is considered (B2b). At this point, overestimation of the bottom friction is found to dissipate wave energy at lower frequencies restricting the peak period to values

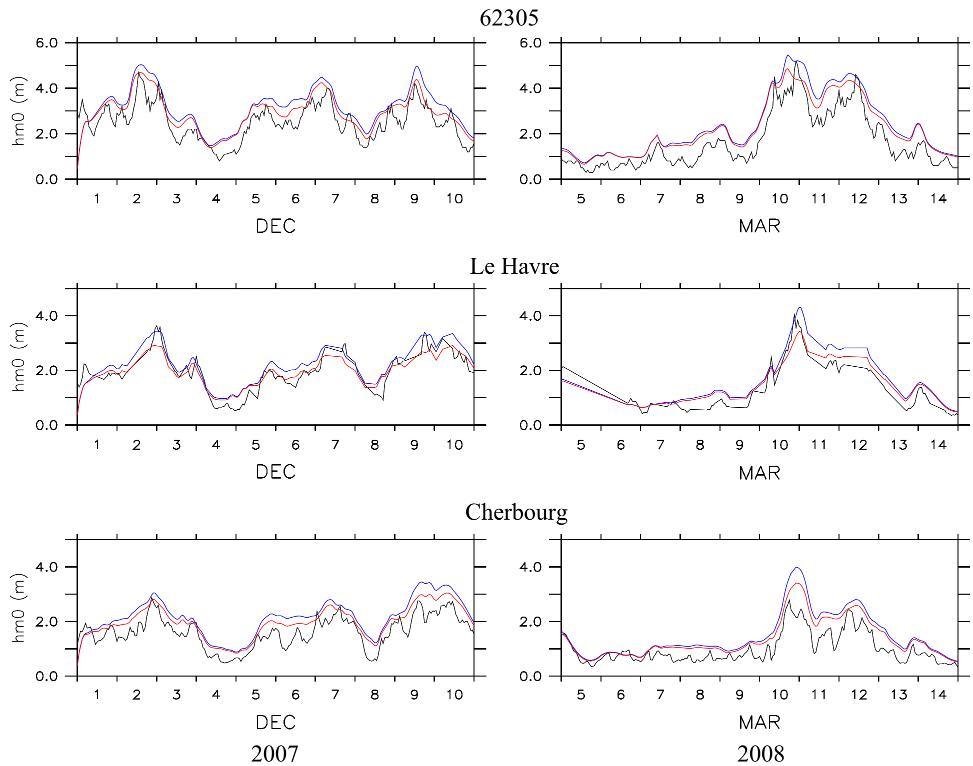


**Fig. 9.** Time series of the significant wave height (black line) observed and predicted in configurations (blue line) B1 and (red line) B3c at lightship 62305 and wave buoys of Le Havre and Cherbourg in December 2007 and March 2008. (For interpretation of the references to colour in this figure caption, the reader is referred to the web version of this paper.)

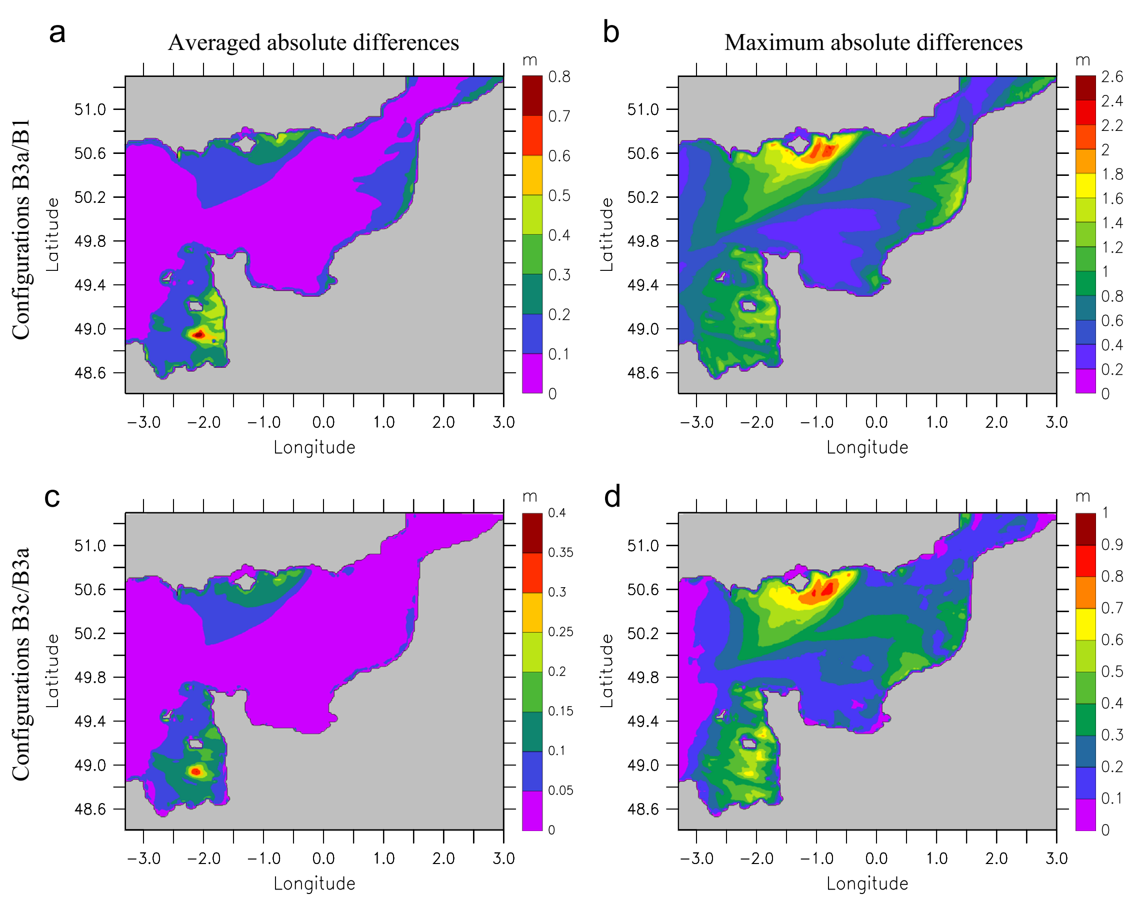


**Fig. 10.** (Left) Averaged and (right) maximum absolute differences between significant wave heights predicted from configurations (top) B3a and B1 and (bottom) B3c and B3a in December 2007–March 2008.

around 8 s. These differences are thus reduced when restricting the computation of statistical parameters to peak period below 8 s (Fig. 8c and d). Predictions obtained with the heterogeneous roughness magnitude are however of a medium quality between numerical results obtained with configurations B1 and B2b. The high sensitivity of peak period predictions at the wave buoy of Le Havre suggests as denoted previously in Section 3.2.1 a combined influence of swell and locally generated wind sea at this measurement point.

In each case, moderate impact of sand ripples (B3c) is obtained at the three measurement sites exhibiting a rather significant effect of macro-roughness variations associated with the transition between areas of sands and pebbles and gravels in the English Channel.

### 3.3. Regional effects of bottom friction

Numerical predictions are exploited further to encompass the spatial and temporal changes of the significant wave height in relation to the integration of the spatial heterogeneous bottom roughness length scale. Fig. 10a and b displays the averaged and maximum absolute differences between significant wave heights predicted from configurations B3a and B1. Significant differences are exhibited in nearshore areas exposed to the incoming waves from the North Atlantic ocean: the Normano-Breton Gulf, the surrounding of the Isle of Wight and the region off the "Pays-de-Caux". Strongest differences over 2 m are obtained at the eastern extend of the Isle of Wight preferentially exposed to the incoming waves through the Hurd deep bathymetric depression in the eastern English Channel (Fig. 2). Similar spatial distributions of wave height modifications are obtained by integrating the heterogeneous bed roughness length scale (B3c) (Fig. 10c and d) mainly as the exposed areas are covered globally by pebbles and gravels (Vaslet et al., 1979; Larsonneur et al., 1982) with strongest $k_n$ values up to 16 cm (Fig. 3). Whereas differences are weaker than between configurations B1 and B3a, the predicted significant wave height experiences modifications up to 1 m in the eastern extend of the Isle of Wight (Fig. 10d). Bottom friction appears furthermore to have on average a moderate effect in water depths over 15 m restricting the differences in predicted wave height below 0.1 m. Stronger modifications are however liable to occur during storm events with maximum absolute differences up to 0.8 m as exhibited at the three measurement points considered (Section 3.2.2).

Further investigations are conducted on the variation of the associated bottom-friction coefficient $C_b$. Fig. 11 displays the spatial distribution of the averaged $C_b$ values from configurations B3a and B3c in December 2007–March 2008. Over much of the computational domain, values obtained with a constant uniform bottom roughness length scale ($k_n = 0.05$ m) (B3a) falls in the range [0.02 m$^2$ s$^{-3}$; 0.08 m$^2$ s$^{-3}$] of constants values prescribed by Hasselmann et al. (1973) ($C_b = 0.038$ m$^2$ s$^{-3}$) and Bouws and Komen (1983) ($C_b = 0.067$ m$^2$ s$^{-3}$) (Fig. 11a). Whereas the integration of the heterogeneous roughness length scale (B3c) slightly modifies the averaged bottom-friction coefficient in the eastern English Channel (Fig. 11b), significant variations are exhibited in nearshore exposed areas of gravels and pebbles where the averaged $C_b$ values are increasing over 0.16 m$^2$ s$^{-3}$. In spite of a relative success of constant empirical coefficients exhibited by Tolman (1994), $C_b$ appears here to experience significant variations with values liable to be between 2 and 4 times greater than the constant empirical coefficient of Bouws and Komen (1983).

## 4. Conclusions

The wave propagation model SWAN has been set up in the English Channel and the southern North Sea to investigate the effects of a heterogeneous bottom roughness length scale on energy dissipation by bottom friction. Numerical results have been compared with available in situ measurements of the significant wave height and the peak period at three offshore lightships and two nearshore wave buoys off Le Havre and Cherbourg harbours. The main outcomes of the present study are the following:

1. Numerical predictions appear to be sensitive to the formulation of the wind-drag coefficient $C_d$. The new formulation recently established by Zijlema et al. (2012) to fit a set of observations at high wind speeds is found to give globally better estimates than the expression of Wu (1982) retained by default in SWAN.
2. Whereas predictions at measurement points show on average a slight sensitivity to bottom friction, differences are exhibited during storm events with overestimation of the significant wave height liable to reach 22% by neglecting the dissipation of wave energy by bottom friction.
3. The integration of the heterogeneous bottom roughness length scale associated with the grain-size distribution of bottom sediments improves the numerical estimates at the point 62305 and the wave buoy of Cherbourg. Sand ripples appear however to have a moderate effect exhibiting a major impact of the macro bottom types of seabed sediments between areas of (1) sands and (2) pebbles and gravels on waves at the scale of the English Channel.
4. The combined effect of hydrodynamics and bed-sediment properties in the formulation of Madsen et al. (1988) is leading to a significant spatial variation of the bottom-friction coefficient $C_b$ particularly noticeable in areas of pebbles and gravels exposed to the incoming waves. This result exhibits the

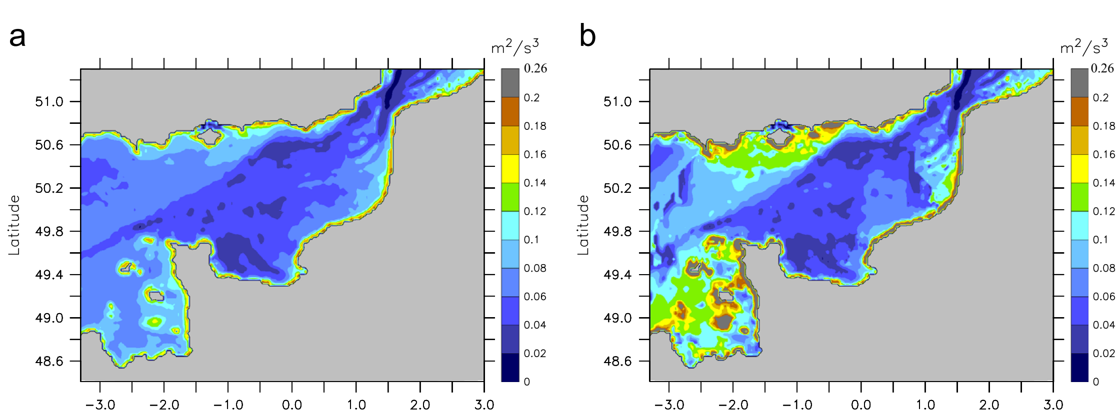


**Fig. 11.** Averaged bottom-friction coefficients predicted from configurations (a) B3a and (b) B3c in December 2007–March 2008.

limitations of constant empirical values suggested by Hasselmann et al. (1973) and Bouws and Komen (1983).

The present study provides thus interesting insights into the effects of wave-energy dissipation by bottom friction on wind-generated surface-gravity waves in the English Channel, its dependency with the formulation of wind drag and the parameterisation of bottom roughness length scale. This research will benefit from extending comparisons of numerical predictions with measurements in the Normano-Breton Gulf and the surrounding of the Isle of Wight as these areas appear preferentially impacted by energy dissipation by bottom friction. Another prospective will consist in integrating the effects of the tide in waves computation and the generation of waves and current sand ripples. These results will help to improve the computation of nearshore waves conditions along the English and French coastlines of the English Channel of utmost interest for numerous coastal engineering applications.

## Acknowledgements

The author is particularly grateful to Météo-France for supplying wind fields data obtained with the meteorological model ALADIN and Dr. Fabrice Ardhuin (Institut Français de Recherche pour l'Exploitation de la MER, France) for giving access to wave data issued from regional runs of WaveWatch III in the curse of the IOWAGA project. Measurements of the significant wave height were provided by the UK Meteorological Office (http://www.metoffice.gov.uk/) and the French CANDHIS database (Cerema) (http://candhis.cetmef.developpement-durable.gouv.fr/). Simulations were performed on computer facilities CAPARMOR (CAlcul PARallèle Mutualisé pour l'Océanographie et la Recherche). The present paper is a contribution to the research program of the Laboratory of Coastal Engineering and Environment (http://memphys-lgce.fr.ht).

## References

Ardhuin, F., O'Reilly, W.C., Herbers, T.H.C., Jessen, P.F., 2003a. Swell transformation across the continental shelf. Part I: attenuation and directional broadening. J. Phys. Oceanogr. 33, 1921–1939.
Ardhuin, F., Herbers, T.H.C., Jessen, P.F., O'Reilly, W.C., 2003b. Swell transformation across the continental shelf. Part II: validation of a spectral energy balance equation. J. Phys. Oceanogr. 33, 1940–1953.
Battjes, J., Janssen, J., 1978. Energy loss and set-up due to breaking of random waves. In: Proceedings of the 16th International Conference of Coastal Engineering, Hambourg, pp. 569–587.
Bénard, P., 2004. ALADIN-NH/AROME dynamical core; status and possible extension to IFS. In: Proceedings of the ECMWF Seminar, pp. 27–40.
Benoit, M., Lafon, F., 2004. A nearshore wave atlas along the coasts of France based on numerical modeling of wave climate over 25 years. In: Proceedings of the 29th International Conference on Coastal Engineering, USA, pp. 714–726.
Bertotti, L., Cavaleri, L., 1994. Accuracy of wind and wave evaluation in coastal regions. In: Proceedings of the 24th International Conference of Coastal Engineering, ASCE, pp. 57–67.
Booij, N.R.C., Ris, R.C., Holthuijsen, L.H., 1999. A third generation wave model for coastal regions, part 1, model description and validation. J. Geophys. Res. 104 (C4), 7649–7666.
Bouws, E., Komen, G.J., 1983. On the balance between growth and dissipation in an extreme, depth-limited wind-sea in the southern North Sea. J. Phys. Oceanogr. 13, 1653–1658.
Cabioch, L., Gentiel, F., Glacon, R., Retière, C., 1977. Le macrobenthos des fonds meubles de la Manche: distribution générale et écologie. In: Keegan, B.F., Ceidigh, P.J., Caston, P.J. (Eds.), Biology of Benthic Organisms. Pergamon Press, Oxford, pp. 115–128
Collins, J.I., 1972. Prediction of shallow-water spectra. J. Geophys. Res. 77 (15), 2693–2707.
Graber, H.C., Madsen, O.S., 1988. A finite-depth wind-wave model. Part I: model description. J. Phys. Oceanogr. 18, 1465–1483.
Guillou, N., 2007. Rôles de l'hétérogénéité des sédiments de fond et des interactions houle-courant sur l'hydrodynamique et la dynamique sédimentaire en zone subtidale—applications en Manche orientale et à la pointe de la Bretagne (Ph.D. thesis in Physical Oceanography). Université de Bretagne Occidentale. Available at ⟨http://tel.archives-ouvertes.fr/tel-00376679/en/⟩, 469 pp.
Guillou, N., Chapalain, G., Thais, L., 2009. Three-dimensional modeling of tide-induced suspended transport of seabed multicomponent sediments in the eastern English Channel. J. Geophys. Res. 114, C07025.
Guillou, N., Chapalain, G., 2010. Numerical simulation of tide-induced transport of heterogeneous sediments in the English Channel. Cont. Shelf Res. 30 (7), 806–819.
Hasselmann, K., Collins, J.I., 1968. Spectral dissipation of finite-depth gravity waves due to turbulent bottom friction. J. Mar. Res. 26, 1–12.
Hasselmann, K., Barnett, T.P., Bouws, E., Carlson, H., Cartwright, D.E., Enke, K., Ewing, J.A., Gienapp, H., Hasselmann, D.E., Kruseman, P., Meerburg, A., Muller, P., Olbers, D.J., Richter, K., Sell, W., Walden, H., 1973. Measurements of wind-wave growth and swell decay during the Joint North Sea Wave Project (JONSWAP). Dtsch. Hydrogr. Z. Suppl. 12 (A8), 1–95.
Hasselmann, K., 1974. On the spectral dissipation of ocean waves due to white-capping. Bound. Layer Meteorol. 1–2 (6), 107–127.
Jonsson, I.G., 1966. Wave boundary layers and friction factors. In: Proceedings of the 10th Conference on Coastal Engineering, Tokyo, Japan, ASCE, pp. 127–148.
Jonsson, I.G., Carlsen, N.A., 1976. Experimental and theoretical investigations in an oscillatory turbulent boundary layer. J. Hydraul. Res. 14, 45–60.
Komen, G.J., Hasselmann, S., Hasselmann, K., 1984. On the existence of a fully developed wind–sea spectrum. J. Phys. Oceanogr. 14, 1271–1285.
Komen, G.J., Cavaleri, L., Donelan, M., Hasselmann, K., Hasselmann, S., Janssen, P.A.E.M., 1994. Dynamics and Modelling of Ocean Waves. Cambridge University Press p. 532
Larsonneur, C., Bouysse, P., Auffret, J.P., 1982. The superficial sediments of the English Channel and its western approaches. Sedimentology 29, 851–864.
Leprêtre, A., Chapalain, G., Carpentier, P., 2006. Une méthode d'interpolation des caractéristiques granulométriques des sédiments superficiels. Bull. Soc. Géol. France 177 (2), 89–95.
Li, M.Z., Amos, C.L., 1998. Predicting ripple geometry and bed roughness under combined waves and currents in a continental shelf environment. Cont. Shelf Res. 18, 941–970.
Li, M.Z., Amos, C.L., 2001. SEDTRANS96: the upgraded and better calibrated sediment-transport model for continental shelves. Comput. Geosci. 27, 619–645.
Luo, W., Monbaliu, J., 1994. Effects of the bottom friction formulation on the energy-balance for gravity-waves in shallow-water. J. Geophys. Res. 99 (C9), 18501–18511.
Madsen, O.S., Poon, Y.-K., Graber, H.C., 1988. Spectral wave attenuation by bottom friction: theory. In: Proceedings of the 21st International Conference on Coastal Engineering, ASCE, pp. 492–504.
Mei, C.C., 1983. The Applied Dynamics of Ocean Surface Waves. Wiley, New York p. 740
Riedel, P.,O'Brien, P., Townsend, M., 2005. The effect of ocean swell on the stability of Adelaide's metropolitan beaches. Coastal Living Coast. Institution of Engineers, Australia Adelaide, Australia, Coasts and Ports.
Shemdin, O., Hasselmann, K., Hsiao, V., Heterich, K., 1978. Nonlinear and linear bottom interaction effects in shallow water. In: Farve, A., Hasselmann, K. (Eds.), Turbulent Fluxes through the Sea Surface. Wave Dynamics and Prediction. Plenum Press, pp. 347–372
Siadatmousavi, S.M., Jose, F., Stone, G.W., 2011. The effects of bed friction on wave simulation: implementation of an unstructured third-generation wave model, SWAN. J. Coast. Res. 27 (1), 140–152.
Smith, G.A., Babadin, A.V., Riedel, P., Young, I.R., Oliver, S., Hubbert, G., 2011. Introduction of a new friction routine into the SWAN model that evaluates roughness due to bedform and sediment size changes. Coast. Eng. 58 (4), 317–326.
Soulsby, R., 1997. Dynamics of Marine Sands. H.R. Wallingford p. 249
SWAN team, 2009. n SWAN Cycle III. Version 40.72 AB—Scientific and Technical Documentation. Technical Report, Delft University of Technology, 107pp.
Tolman, H.L., 1991. A third-generation model for wind waves on slowly varying unsteady, and inhomogeneous depths and current. J. Phys. Oceanogr. 21, 782–797.
Tolman, H.L., 1994. Wind-waves and moveable-bed bottom friction. J. Phys. Oceanogr. 24, 994–1009.
Van Rijn, L.C., 1993. Principles of Sediment Transport in Rivers, Estuaries and Coastal Seas. Aqua Publications, Amsterdam, 6–5.
Vaslet, D., Larsonneur, C., Auffret, J.P., 1979. Map of the surficial sediments in the English Channel, scale 1:500,000. Bureau de Recherches Géologiques et Minières, Orléans, France.
Weber, S.L., 1991a. Eddy-viscosity and drag-law models for random ocean wave dissipation. J. Fluid Mech. 232, 73–98.
Weber, S.L., 1991b. Bottom friction for wind sea and swell in extreme depth-limited situations. J. Phys. Oceanogr. 21, 149–172.
Willmott, C.J., 1981. On the validation of models. Phys. Geogr. 2 (2), 219–232.
WISE Group, 2007. Wave modelling—the state of the art. Prog. Oceanogr. 75, 603–674.
Wooding, R.A., Bradley, E.F., Marshall, J.K., 1973. Drag due to regular arrays of roughness elements of varying geometry. Bound. Layer Meteorol. 5, 285–308.
Wu, J., 1982. Wind-stress coefficients over sea surface from breeze to hurricane. J. Geophys. Res. 87 (C12), 9704–9706.
Yalin, M.S., 1985. On the determination of ripple geometry. J. Hydraul. Div. 8 (111), 1148–1155.
Zijlema, M., van Vledder, G.Ph., Holthuijsen, L.H., 2012. Bottom friction and wind drag for wave models. Coast. Eng. 65, 19–26.